Tailored pseudopotentials for magnesium surface core level shift calculations

Tailored pseudopotentials for magnesium surface core level shift calculations

Zhe Xing [1], Dmytro Orlov [1], and Elsebeth Schröder [2,*]

[1] *Division of Mechanics, Materials and Component Design (MMC), Department of Industrial and Mechanical Sciences, LTH, Lund University, Box 118, SE-22100 Lund, Sweden*

[2] *Microtechnology and Nanoscience, MC2, Chalmers University of Technology, SE-41296 Göteborg, Sweden*

(Received 21 September 2024; accepted 15 November 2024; published 3 December 2024)

In x-ray photoelectron spectroscopy (XPS), identifying the origin of peaks in the spectrum can be guided by theory calculations. With density functional theory (DFT), using pseudopotentials, one can obtain the difference in photoelectron energy for electrons originating from atoms of different environments, for example surface and bulk atoms, and thus model the surface core level shift (SCLS) energies. The focus in this work is to prepare for calculations of magnesium (Mg) $2p$ SCLSs in material systems where dispersion interactions play a role, primarily in Mg surface degradation and adsorption of molecules as relevant, for example, in degradable bioimplants. For SCLS DFT calculations in metallic surfaces, the state of the photoelectron must be treated as a core state. In the case of Mg, standard pseudopotentials treat the $2p$ state as a valence state, not a core state. We therefore need Mg pseudopotentials with the $2p$ electrons in the core, leaving only two electrons for the valence region (the $3s$ electron); Two-valence electron pseudopotentials are not common, because DFT calculations of Mg-containing materials usually are better or more easily described using 10 valence electrons. In this work, new two-electron Mg pseudopotentials are therefore created for use in dispersion-inclusive DFT calculations. To our knowledge, no such two-electron Mg pseudopotentials exist, proven to work well with the nonlocal, dispersion-inclusive, exchange-correlation functional vdW-DF-cx or similar functionals. We create a number of two-electron Mg pseudopotentials and their $2p$-hole partners, and for four of the most promising we assess their performance in vdW-DF-cx. We provide results for Mg and MgO bulk phases and for the Mg(0001) surface energy, structure, and SCLS, and where possible we compare with results that we obtain by using conventional 10-electron Mg pseudopotentials, all-electron calculations, and with experiments. This work not only reports and tests the specific conditions for creating $2p$ Mg results, it will also, we believe, be of help in creating other similar pseudopotentials to aid the analysis of XPS spectra in other materials.

DOI: 10.1103/PhysRevMaterials.8.123801

I. INTRODUCTION

For atomic-scale theory calculations of solid materials, density functional theory (DFT) is a useful tool for analyzing and evaluating basic properties such as lattice constants, atomic positions, and electron charge densities. In analyzing x-ray photoelectron spectroscopy (XPS) spectra of surfaces and molecules, DFT calculations of core level shifts can be of help in identifying the origin and position of peaks in the spectra.

In DFT, for ease of the computational burden, pseudopotentials (PPs) must typically replace the details of the core electric states of the atoms, resulting in fewer nodes in the valence electron wave functions and thus simpler calculations.

A popular method for calculating surface core level shifts (SCLSs) from metallic surfaces is based on the change in total energies when a core electron is removed in the same atomic species in two different positions, one of them typically in a bulklike position, the other in a surface position. In DFT with PPs, two versions of the PP are then needed: an ordinary version, where the orbital of the relevant electron is in the core part of the PP, and a PP that is identical except that the orbital now lacks one electron (has a hole) in that orbital [1].

While DFT in itself is an exact theory, directly mapped from the Schrödinger equation for the full system, it is always necessary to approximate the exchange-correlation (XC) part of the system total energy. In materials with sparse regions, be it voids, layers, or space between a surface and an adsorbed molecule, it is important that the approximations of the XC energy functional in DFT do not approximate away the long-range interactions, such as the dispersion interactions. While solid bulk and surfaces without adsorbants may be well described by semilocal approximations, such as the generalized gradient approximations (GGAs), those approximations are invalid for systems in which dispersion interactions are significant.

Here, we focus on magnesium (Mg) and its energetically most favorable surface Mg(0001). Magnesium is a light energy-saving material, critical applications of which in biomedicine, energy storage, and light-weight mobility depend heavily on an in-depth understanding of surface

*Contact author: schroder@chalmers.se

reactivity. For this reason, in future work we would like to study also the interactions of molecules with Mg and Mg alloy surfaces, and layered degradation-related phases with Mg, such as $Mg(OH)_2$.

The surface energy and the structure of Mg(0001) and its SCLSs for Mg-2p electrons were previously evaluated in DFT within GGA by use of the Perdew-Burke-Ernzerhof (PBE) exchange-correlation (XC) functional [2] and a set of PBE-based Mg PPs with and without a hole in the 2p orbital [3,4]. While GGA is likely sufficiently accurate for most surface calculations of the metal, for use in corrosion and molecular adsorption studies the dispersion interactions become important, and an approximate XC with awareness of the dispersion interaction must be chosen. It has also been shown that dispersion interactions are crucial in describing ionic crystals [5–10], which means that as the Mg surfaces start to oxidate, PBE describes the system less accurately. We therefore turn to the vdW-DF-cx [11,12] functional, which includes the dispersion interactions and which has been documented to work well both for surfaces and in physisorption problems [10,13–17].

In general, it is advisable to use PPs created with the same XC functional as used in the DFT calculation. For the previous PBE calculations of SCLS in Mg(0001) [3,4], PBE-based PPs were used, created in the `ld1.x` code within the Quantum Espresso suite [18–20]. We explore here whether we need to use different PPs in vdW-DF-cx calculations. Ideally, we would create PPs based on vdW-DF-cx. However, the vdW-DF-cx functional is not available in `ld1.x` and instead we focus on other XC choices that are similar to vdW-DF-cx.

In the present work, we thus create a set of new Mg PPs with two valence electrons, including their 2p hole variants, we discuss and evaluate both the existing set of PPs and the new PPs for basic bulk and surface properties, and we compare Mg and MgO phase results to new all-electron results also presented here. We also evaluate the PPs in SCLS calculations.

In the following, we first discuss the use of PPs in DFT, and we introduce the methods used in PP generation, the PP DFT calculations, the SCLS evaluations, and the all-electron calculations. We then continue with a description and discussion of the results, of which a selection is presented here while a fuller set is presented in the Supplemental Material [21]. We compare our results of using two-electron PPs with previous calculated and measured results, where available, with our results of using Mg PPs with 10 valence electrons, and with all-electron calculations created here. We show that the PBE ad hoc hole-PP of Ref. [3] is satisfactory for use with PBE calculations of the type considered here, and we make an informed choice of PPs that we will use with vdW-DF-cx in future work. Further, we study which of the properties are most influenced by changes in the DFT XC choice and the choice of PP.

II. THE NEED FOR CREATING FURTHER PSEUDOPOTENTIALS

The present work is part of a larger study in which XPS spectra of 2p electrons from Mg surfaces are obtained. In XPS measurements, the radiation kicks out an electron from (here) the 2p orbital in one of the Mg atoms, leaving a hole (missing electron) in that 2p orbital, which is not filled within the timescale considered. The energy of the expelled electron will depend not only on the orbital it came from (here 2p, but it could also be, e.g., 2s), but also on the chemical environment of the atom, for example whether it is a surface or bulk atom. The SCLS is the measured energy difference between an electron from the same orbital of a Mg atom in the surface and in bulk.

We calculate DFT-based estimates of the SCLS by assuming that after the removal of the Mg 2p electron from an atom, the remaining core electrons are unaffected, while the valence electrons relax fully to accommodate the hole in the 2p orbital. The SCLS is then calculated as the total energy difference between having the 2p hole in a surface Mg atom, and having the hole in the bulk of the material [1].

In PPs for use in DFT calculations, the (full) potential of the core electron is replaced by an effective potential, the pseudopotential, describing the details of the interaction of valence electrons with the core electrons. The lower panel in Fig. 1 illustrates the radial part of this effective potential compared to the full potential, for one of our two-electron PPs. Beyond the distance r_{loc} they are identical. While the valence electrons are still fully described in the valence region, and their density is free to adjust according to the fields working on them, the PP replacement results in faster calculations because the modified valence electron wave functions Ψ_{nl} have fewer nodes, as illustrated in the upper panel of Fig. 1 for the radial part of the 3s and 3p orbitals. Beyond the radius r_{cut} the pseudo-wave-functions are identical to the full wave functions.

In SCLS calculations, to prevent other electrons from filling the hole during the optimization of the electron distribution, we need to include the 2p orbitals among the core electrons of the Mg PP. This leaves only two electrons (in an isolated Mg atom these would be the 3s electrons) as valence electrons in the PP description. Describing Mg-based material properties well with a Mg PP that only has two valence electrons is a challenge, but not impossible [3,4,22,23].

Usually, Mg PPs are created with 10 valence electrons (thus including the electrons of the 2s and 2p orbitals in the valence electron description) and only the 1s electrons in the core description. This is known, in general, to give better descriptions of Mg surfaces, bulk, and alloys, compared to similar (often older) PPs with two valence electrons. We therefore need to be careful when choosing or designing both the Mg PP and its 2p-hole companion.

For the initial DFT calculations [4] we took over a two-valence electron Mg PP and its ad hoc created 2p-hole version, created specifically for a previous study [3]. This pair of PPs is based on PBE and created for use in PBE-based DFT calculations. We call them here Mg-pbe-us-3d and Mg-pbe-us-3d-h; full file names for all PPs used here are listed in Table I. The pair gives reasonable results for PBE-based Mg surface calculations, both ordinary calculations (such as lattice constants, surface energies, surface atom relaxations) and SCLS calculations, as shown in Refs. [3,4] and the present work. However, for use in DFT calculations with other XC

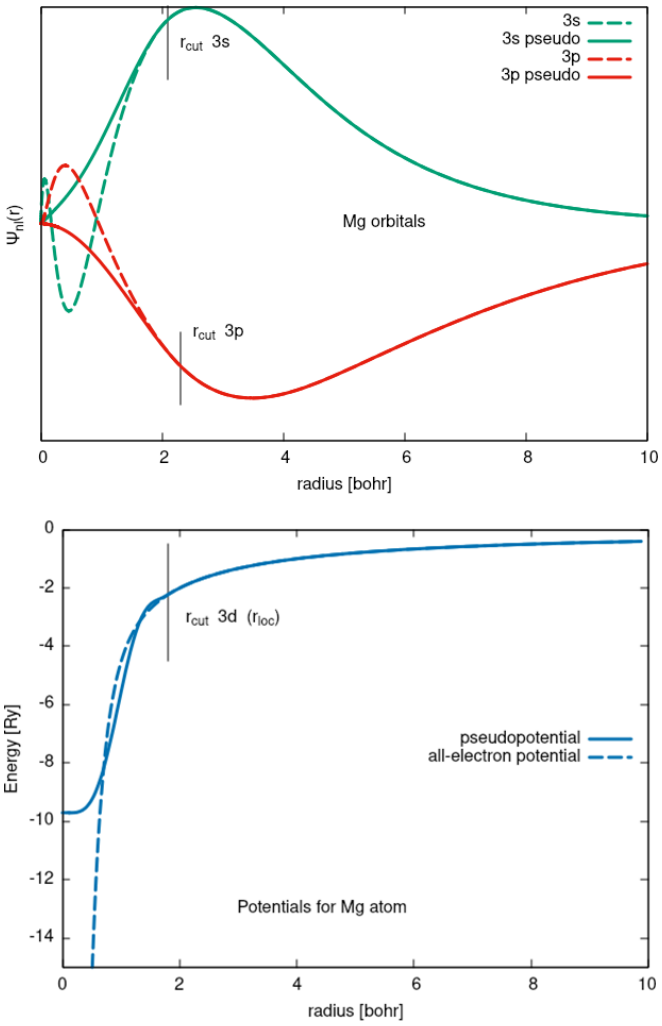

FIG. 1. Top panel: All-electron and pseudo-wave-functions for Mg orbitals 3*s* and 3*p*. Radii for smooth transitions from core to valence regions in the 3*s* and 3*p* wave functions are indicated; the pseudo-wave-functions have fewer nodes than the full wave functions. Bottom panel: All-electron and pseudopotential. The nonlocal core correction part of the pseudopotential is not included in the plot. In this pseudopotential, the 3*d* orbital is chosen as the local reference state, and the position of the smooth transition in the potential ($r_{\rm loc}$) is identical to the smooth-transition radius for the 3*d* wave function ($r_{\rm cut}$ for 3*d*). All curves are for the pseudopotential Mg-pbesol-paw-3d.

approximations than PBE, we cannot assume *a priori* that this set of PBE-based PPs will work well.

As mentioned above, we need an XC approximation in the DFT calculations that does not approximate away dispersion interactions. The vdW-DF [11–15,27] family of functionals fulfills this need, and they are by now well-tested and established functionals. We use here the consistent-exchange [12] version vdW-DF-cx. However, because no PP creation codes to date include the vdW-DF as a choice of XC functional, we explore whether the PBE-based PP from Ref. [3] is sufficiently accurate also with vdW-DF-cx, and we create and test new two-valence electron Mg PPs that are based on other relevant XC functionals.

TABLE I. Pseudopotentials (PPs) used in the present work, and their file names. When not stated with "10e," the Mg PPs presented here have two valence electrons. The "-3d" denotes PPs in which the 3*d* state is chosen to be the local reference state, while other PPs pseudize the all-electron potential. The Mg-2p-hole versions of the Mg PPs have a "-h" added to the name (not shown). The "-gbrv" PPs are from the GBRV library [24], version 1.5, while other O and 10-valence electron Mg PPs are from PSLibrary [25,26], version 1.0.0.

Name here	Full file name
Mg-pbe-us-3d	Mg.pbe-nl-rrkjus.UPF
Mg-cx13pbe-paw-3d	(this work)
Mg-pbesol-us	(this work)
Mg-pbesol-paw	(this work)
Mg-pbesol-paw-3d	(this work)
Mg-pbe-us-10e-3d	Mg.pbe-spnl-rrkjus_psl.1.0.0.UPF
Mg-pbesol-paw-10e-3d	Mg.pbesol-spnl-kjpaw_psl.1.0.0.UPF
Mg-pbesol-us-10e-gbrv	mg_pbesol_v1.4.uspp.F.UPF
O-pbe-us	O.pbe-n-rrkjus_psl.1.0.0.UPF
O-pbesol-paw	O.pbesol-n-kjpaw_psl.1.0.0.UPF
O-pbesol-us-gbrv	o_pbesol_v1.2.uspp.F.UPF

While it would be convenient to have access to a full library of (well-tested) hole-PPs for holes in all possible core orbitals of the various elements, no such library exists, and in reality we need to create hole-PPs on a case-by-case basis. We show here that the above PBE-based PP from Ref. [3] works reasonably well with vdW-DF-cx, but is not as accurate (compared with 10-valence electron PPs and all-electron calculations) with vdW-DF-cx as it is with its native PBE XC. We create new PPs specifically for use with the vdW-DF-cx functional, making minimal changes to the PBE-based PP, and we test those with vdW-DF-cx.

III. METHODS

In this project, we create two-electron Mg PPs, test them in DFT calculations, calculate 10-electron and all-electron bulk lattice constants and energies for comparison, and calculate SCLSs for the Mg(0001) surfaces using the PPs and their hole companions. We describe here the methods used for PP creation, for the PP DFT calculations, for the all-electron DFT calculations, and for SCLS calculations, and we discuss the (lack of) experimental results at low temperatures.

Successful PPs must work for compact metal structures such as bulk and surfaces, in oxides, and in systems where dispersion is dominant, for example in physisorption problems. Our focus here is on testing the PPs on compact metal and oxide structures, using PPs based on XC choices where at least the exchange part is known to act reasonably in systems where dispersion interactions prevail.

It is important to distinguish the use of XC in creation of the PPs, and the XC used in the DFT calculations. As mentioned, the ideal situation has the same XC choice in both. We focus on vdW-DF-cx for the DFT calculations, testing also PBE DFT calculations, but because we cannot use vdW-DF-cx as XC in the PP creation, we instead test a number of other reasonable choices of XC for the PPs. It is also important to note that both the XC choice in DFT and the XC choice (and

```
&input
title='Mg', zed=12., config='1s2 2s2 2p6 3s2 3p0 3d-1',
rel=1, iswitch=3, dft='PBEsol'
/
&inputp
author='ES', lpaw=.true., pseudotype=3,
file_pseudopw='Mg-pbesol-paw-3d.UPF', lloc=2, tm=.true.,
which_augfun='PSQ', rmatch_augfun_nc=.true., nlcc=.true.,
new_core_ps=.true., rcore=1.8
/
5
3S  1  0  2.00  0.00  1.90  2.10  0.0
3S  1  0  0.00  6.00  1.90  2.10  0.0
3P  2  1  0.00  0.00  2.10  2.30  0.0
3P  2  1  0.00  3.50  2.10  2.30  0.0
3D  3  2  0.00  1.00  1.80  1.80  0.0
/
```

FIG. 2. Input file for pseudopotential creation in `ld1.x`, here a two-valence electron Mg PBEsol PAW pseudopotential without a core hole.

other parameter choices) in the PP creation may affect our results, and we focus here on how the PPs affect results, but we mention also the differences we observe between vdW-DF DFT calculations and PBE DFT calculations.

A. Creation of pseudopotentials

We create our new pseudopotentials using the `atomic` (`ld1.x`) program, versions 6.5 and 7.1, under the Quantum Espresso suite [18–20]. The Mg PP provided to us from the study in Ref. [3] was also created in `ld1.x`, although using an earlier (5.2.1) version. Within this text, we refer to the pseudopotentials by abbreviated systematic names; Table I lists the names of PPs and their file names when not from this work, including PPs with 10 valence electrons used for the comparisons and O PPs for use in the MgO bulk calculations.

For the PP creation, we follow the instructions of `atomic`, including the recommended checks for ghost states, transferability, and other possible errors and warnings. Here we only discuss a smaller selection of these initial tests, and we focus the further testing mainly on the behavior in materials.

Figure 2 contains the input file to `ld1.x` for one of our Mg PPs, namely Mg-pbesol-paw-3d. Like the PP Mg-pbe-us-3d of Ref. [3], all our new PPs presented here are either ultrasoft [28] (US) or use the closely related projector augmented waves [29] (PAWs) as a representation of the valence electron interaction with the core electrons. We do not attempt to create norm-conserving PPs as they require in general higher energy cutoff values in the DFT calculations, and our ultimate goal is to use the PPs in calculations with many hundreds of Mg atoms, which would be too computationally expensive. All the PPs we create use the nonlinear core correction [30] with Bessel functions, Troullier-Martins pseudization of the core [31], and they are scalar-relativistic.

The main differences between the PPs are the choice of XC functional, use of US or PAW, and the electronic reference configuration and the related choice of local channel. With this comes necessary modifications to several of the radii involved in the PP creation; in particular, the hole versions of the PPs are sensitive to the radii, sometimes not passing the initial checks, even if the PP without a hole did. Further, since the Mg atoms will be used in a bulk and surface environment, not as isolated Mg atoms, in some of the PPs we honor the hybridization of the $3s$ and $3p$ orbitals in materials by moving 0.25 electron from the $3s$ to the $3p$ orbital. This is not strictly necessary, but it will help the electron convergence in the DFT calculations.

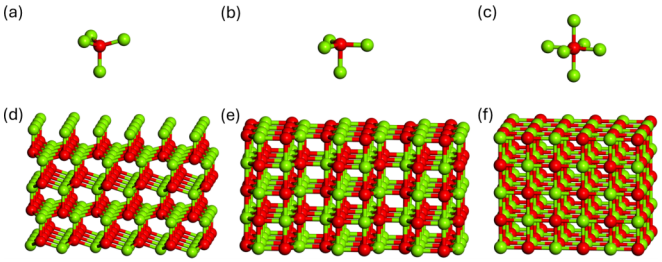

FIG. 3. MgO bulk phases with positions of Mg atoms (green) around the O atom (red) and the full structure of several unit cells, for (a) + (d) wurtzite, (b) + (e) hexagonal-MgO, and (c) + (f) rocksalt.

In short, we systematically test various relevant XC choices, all described in the Results section. We test putting 2 and 0, or 1.75 and 0.25, electrons in the $3s$ and $3p$ orbitals, we test using US and PAW, and we test the choice of local channel. Some of these combinations crash already when using the ld1.x code, and some result in PPs or their hole versions that do not pass the basic sanity checks of being free of ghost states and being transferable, even when elaborating with values of the radii (such at the r_{cut} values) involved. Others give lattice constants of Mg bulk that are unrealistic. The remaining combinations are those we test in this paper.

We would like to emphasize that we do not claim to have optimized the creation of the two-electron Mg PP, which would be rather difficult, given, for example, the sensitivity to choices of the many radii involved. Instead, we find here a couple of PPs that can be used for our purpose, with good results. We make no claims of testing the pseudopotentials as universally usable (e.g., as atoms in molecules, in other surfaces than studied here, in alloys, or as rattler atoms). Our focus is on simple Mg surfaces, their oxidation, and in obtaining SCLSs. We have tailored the PPs we want to use, but another adjustment may have other equally good, or even better, PPs in store.

B. DFT pseudopotential calculations of bulk, surface, and oxide structures

Once the PPs are created, we use DFT to calculate Mg bulk properties in the hexagonally closed packed (hcp), the face centered cubic (fcc), and the body centered cubic (bcc) phases, the surface properties of Mg(0001), as well as properties of MgO bulk phases rocksalt (RS), wurtzite (WZ), and hexagonal-MgO (h-MgO), illustrated in Fig. 3. The two latter metastable phases of MgO are considered here, because we have shown [4,32] that in the initial oxidation of Mg surfaces, the local atomic structure around the O atom is tetragonal, similar to O in the WZ and h-MgO phases [Figs. 3(a) and 3(c)], not octahedral as in the RS phases [Fig. 3(e)].

The DFT calculations are carried out with the plane-wave DFT code `pw.x` of the Quantum ESPRESSO suite [18–20], an open-source implementation of DFT using periodic boundary

conditions and PPs. We use the XC functional vdW-DF-cx [11,12] and for comparison also PBE [2].

The kinetic energy cutoff for the plane waves, used in describing the wave functions and charge densities, are converged for lattice constants of the Mg hcp structure, as well as for the difference in formation energy per atom between phases hcp, fcc, and bcc. Simultaneously, we converge the k-point sampling. For calculations that include O atoms, the cutoff energies and k-point samplings are optimized on the MgO lattice constant of the RS, WZ, and h-MgO phases and the differences in their formation energy. For all k-point samplings in this work, Monkhorst-Pack [33] grids are used.

All calculations are carried out with periodically repeated unit cells. In some systems periodicity is desired, such as the periodicity of Mg and MgO bulk. For the surface calculations, however, to avoid an effect from the periodicity in the direction perpendicular to the surface, we provide 15 Å of vacuum between the images of the surface slabs. When calculating the energy of core holes, the periodicity in the plane of the surface causes the core hole to have several neighbors. To avoid artificial interaction between them, we use a 5×5 Mg(0001) surface unit cell, yielding a surface unit with side lengths, and thus smallest distance to the neighbors, of approximately 16 Å. For a core hole in hcp Mg bulk we use a $5 \times 5 \times 3$ unit cell, again corresponding to approximately 16 Å side lengths in all directions.

In all calculations, except the SCLS calculations, the atom positions are optimized by minimizing the Hellmann-Feynman forces on the atoms, using the BFGS algorithm [34–38]. The convergence thresholds for the total energy and forces are $n_a \times 10^{-8}$ a.u., where n_a is the number of atoms.

For the O atoms in the MgO bulk calculations, we use existing O PPs with six valence electrons, either created from PBE or PBEsol, as a US or PAW potential, Table I; we choose PBE or PBEsol versions according to the accompanying Mg PPs. Two O PPs are obtained from the PSLibrary [25,26] and one from the Garrity-Bennett-Rabe-Vanderbilt [24] (GBRV) library; please refer to Table I for their file names.

For the comparison of the lattice constant and surface relaxation results, we also use three standard Mg PPs with 10 valence electrons, namely the Mg-pbe-us-10e-3d and Mg-pbesol-paw-10e-3d from PSLibrary, and Mg-pbesol-us-10e-gbrv from the GBRV library.

It is well known [39] that surface relaxations in Mg(0001) disturb the positions of the atoms far into the subsurface, and for high accuracy of some of the quantities, a slab of a minimum thickness of 23 Mg atoms, relaxed on both sides, is needed [39]. This is a large calculation in cases when there is also a need for 5×5 copies of the surface unit cell. We therefore also test a slightly thinner slab, at 19 Mg layers, for a couple of the PPs. As we indeed find 19 layers insufficient for describing the relaxations of the Mg(0001) surface accurately, we continue with the 23-layer calculations and instead test the method of lifting off the nine top atomic layers from the 23-layer relaxed slab, keeping the four lowest of them fixed in their relaxed positions found as layers 6–9 in the 23-layer slab. We test the accuracy of this method for the SCLS calculations, as presented in the Results section.

C. All-electron calculations of bulk

We compare our bulk results with 10-valence-electron PP DFT calculations and with all-electron DFT calculations. This way we can study the sensitivity of the PPs without being distracted by possible issues arising from DFT itself and from the XC approximations chosen for the DFT calculations. We use Wien2k, which is an all-electron, full-potential DFT code, using linearized augmented plane waves [40].

Previous all-electron PBE calculations are available for hcp, bcc, and fcc Mg bulk in Ref. [41], but there are no vdW-DF-cx results. For the MgO rocksalt phase, there are PBE and vdW-DF-cx all-electron calculations available, but both calculations are based on a PBE electron density, which means that the vdW-DF-cx calculation is not self-consistent [42]. Thus, due to the lack of data to which we can compare our PP DFT results, we created new all-electron results of lattice constants and total energy differences for Mg and MgO bulk structures with PBE and vdW-DF-cx XC functionals, keeping accuracy in focus.

For the Wien2k calculations, our starting point was the set of parameter choices from the high-accuracy setting in the initialization algorithm. For parameters (such as k-point sampling) with no direct guidance, and for all parameters that we found to influence our results, we carried out convergence studies mainly on the MgO RS and Mg bcc structure with vdW-DF-cx DFT, and we did smaller tests for the other bulk phases to confirm convergence in those phases with the chosen parameter values. Explicitly, for the general parameters we choose $R_{\mathrm{MT}}^{\mathrm{min}} K_{\mathrm{max}} = 8$, $G_{\mathrm{max}} = 25$ bohr^{-1}, $l_{\mathrm{vnsmax}} = 8$, and a factor 4 enhancement in the FFT grid. For the vdW-DF-cx calculations, we choose $G_{\mathrm{maxpot}} = 12$ bohr^{-1}. The muffin-tin radius of the atoms is chosen to be $R_{\mathrm{MT}} = 1.7$ and 2.0 bohr for the O and Mg atoms, respectively. While the RS structure has space for larger radii, the h-MgO structure does not, and in order to compare the total energies of the calculations, we choose the same parameters in all calculations, including the Mg bulk phases. In each of the calculations, the convergence thresholds for total energy and charges are set to 10^{-8} Ry (0.0001 meV) and 10^{-7} e.

For the k-point sampling, we find that Wien2k results are more sensitive to the k-point density than our Quantum Espresso calculations. For the MgO RS bulk primitive structure, we find that a $46 \times 46 \times 46$ mesh is needed for converging the total energy in the energy-versus-lattice-constant curves to obtain lattice constant(s) to the accuracy of 0.001 Å. In comparison, we find in Quantum Espresso that a $10 \times 10 \times 10$ grid suffices for our MgO RS calculations.

To wrap up, for the Wien2k calculations we use $46 \times 46 \times 46k$-points for MgO RS, $40 \times 40 \times 28$ for the h-MgO phase, $150 \times 150 \times 90$ for Mg hcp, and $160 \times 160 \times 160$ for the primitive unitcells of Mg bcc and fcc.

D. References for lattice constants

For evaluating the Mg PPs with two valence electrons, we compare bulk lattice constants of several structural phases of Mg and MgO with results of DFT using 10-electron Mg PPs, with our all-electron calculations, and with experimental data, where available.

Since DFT calculations (PP-based and all-electron) are carried out at zero temperature and do not include zero-point (quantum) fluctuations, it might be reasonable to assume that low-temperature experimental values, back-corrected to zero temperature and no zero-point fluctuations, are more relevant for comparisons than the uncorrected, ambient-condition results. However, we were not able to find low-temperature experimental results for the Mg bulk hcp lattice constants, neither back-corrected to remove zero-point fluctuations (quantum fluctuations) nor results extrapolated to ∼0 K. The experimental lattice constants at 298 K have been measured to be $a = 3.209\,22$ Å and $c = 5.210\,67$ Å (with ratio 1.623 66), obtained from an average over six sources [43]. For the RS phase of MgO, the situation is better. The lattice constant at 19.8 K has been measured to be $a_{\mathrm{MgO}} = 4.207$ Å [44], and corrected for thermal and zero-point motion $a_{\mathrm{MgO}} = 4.186$ Å [45].

The main comparison for the quality of our PPs should therefore instead be with the 10-electron and the all-electron calculations (with the corresponding PBE or vdW-DF-cx choice in the DFT calculations).

E. SCLS calculations

Ultimately, our PPs are created with the purpose of finding SCLSs in clean and slightly oxidized surfaces. The SCLS calculations on clean Mg(0001) test both the PPs and, as the only test here, also their hole companions.

All our SCLS results are based on four calculations for each data point: Mg bulk with ∼16 Å side length with and without one Mg atom of the hole PP, $E_{\mathrm{bulk}}^{5\times5\times3}$, and the surface of interest with and without a Mg hole in the ith layer, $E_{\mathrm{surf},i}^{5\times5}$ also with 16 Å side length in the surface plane. The SCLS is then obtained as the differences

$$\Delta_{i,\mathrm{bulk}} = \left(E_{\mathrm{surf},i}^{*5\times5} - E_{\mathrm{surf},i}^{5\times5}\right) - \left(E_{\mathrm{bulk}}^{*5\times5\times3} - E_{\mathrm{bulk}}^{5\times5\times3}\right), \quad (1)$$

where the star denotes the presence of an Mg atom with a $2p$ hole. The ∼16 Å side lengths in the surface and bulk are obtained by using a 5×5 Mg(0001) surface supercell and a $5 \times 5 \times 3$ hcp bulk supercell.

With the lack of an electron in the system, it is possible that the atoms would move slightly due to the change in electron density, if given enough time. However, electric transitions, such as the creation of a core hole, are much faster than the motion of the atoms, and we therefore calculate the total energy of the system with a core hole as a self-consistent-field calculation. In other words, the electron density is allowed to reorganize due to the sudden lack of an electron, but the atoms are not allowed to move.

IV. RESULTS AND DISCUSSION

As mentioned in the Methods section, we have created a set of new PPs based on a number of XC choices. Several tentative PPs or their hole companions already failed the first initial tests, and they are not mentioned further here, while others turned out to give bulk lattice constants too far off established values, and are similarly discarded. In the end, we settle for three sets of PBEsol PPs and one PP based on the vdW-DF-cx exchange, cx13, and the PBE correlation; see Table I. Three are PAW PPs. For these four PPs, and for the Mg-pbe-us-3d PP of Ref. [3], we carry out further tests here and comparisons of bulk and surface structures, including SCLS calculations.

The goal is to find one or more two-valence electron Mg PPs that are well suited for situations with O adsorption and in calculations for systems in which dispersion matters. We therefore test the PPs in MgO bulk structures of relevant local geometry, with vdW-DF-cx as the XC choice. To evaluate how well the Mg PPs work, we also carry out bulk Mg and MgO DFT calculations with 10-valence electron PPs and all-electron DFT calculations, where the 10-electron results can be seen as an intermediate in the path towards all-electron calculations.

In the following, we first explain some of the choices made in creating the PPs, and we report our testing of the PPs in DFT calculations. Convergence criteria are also tested and determined.

A. Prelude on pseudopotential parameters

1. Exchange-correlation functional

The obvious first choice for creating a new PP, off of an already existing and functioning PP, is to change as little as possible. For our use, we change the XC upon which the PP is based because our DFT calculations will change from using PBE in Ref. [4] to using vdW-DF-cx in future work.

For our new sets of PPs, we studied a range of relevant XC functionals on which to base the PPs for this purpose, and we ended up further testing PPs based on the PBEsol, the B86bPBE, and the $\mathrm{cx13} + \mathrm{PBE}_{\mathrm{corr}}$ XC functionals, as well as the Mg-pbe-us-3d of Ref. [3]. The latter is optimized for the PBE exchange-correlation functional, and it has not previously been tested with the vdW-DF-cx functional.

In GGA-type functionals, the exchange enhancement factor $F_x(s)$, as a function of the reduced electron density gradient $s = |\nabla n| n^{-4/3} (24\pi^2)^{-1/3}$, scales the exchange energy and defines the nature of the exchange, Fig. 4. The vdW-DF-cx is not a GGA functional, because the correlation part includes nonlocal contributions, but the exchange part of vdW-DF-cx, here called cx13, is a GGA exchange combined from the Langreth-Vosko (LV) screened exchange [46] at small s, bridged to the revised Perdew-Wang-86 [47,48] (rPW86) from around $s \approx 2.5$. We can thus create PPs with the exchange of vdW-DF-cx, cx13, but we will have to choose a different correlation part.

Typical values of s for the shorter-range systems tested here are less than 2, while molecular adsorption problems, relevant in future work, typically include also larger values of s, due to the more abrupt changes in electron density outside of the molecules (numerator in s) combined with small electron densities (denominator in s). For our future work, we need PPs that work well both for small and larger values of s. The tests of this work focus on bulk and surfaces, at smaller s values. Besides passing our bulk-related tests here, good PPs for our future work will also need to be well behaved at larger values of s and have correlation that works reasonably with vdW-DF-cx in DFT calculations.

Figure 4 shows the $F_x(s)$ of a number of relevant exchange functionals. If everything were determined from exchange only, then cx13 would be the ideal choice for exchange in a PP

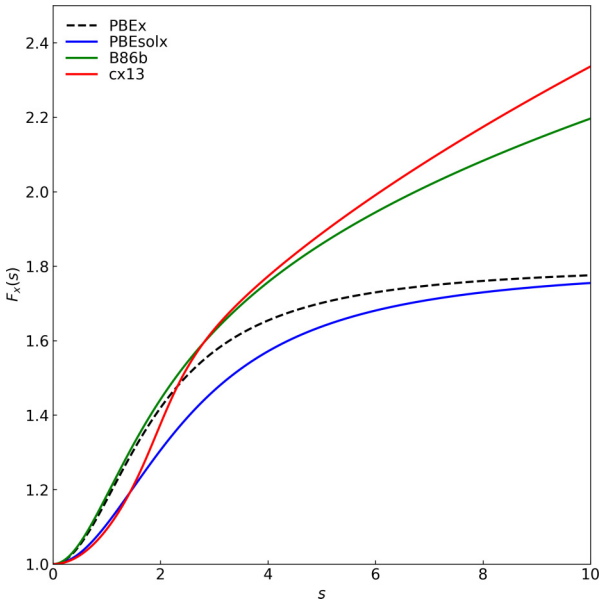

FIG. 4. Exchange enhancement factor $F_x(s)$ for the exchange choices mentioned here. $F_x(s)$ scales the exchange from that of the local density approximation, at $F_x(s) = 1$, as a function of the reduced electron density gradient $s = |\nabla n|n^{-4/3}(24\pi^2)^{-1/3}$.

for vdW-DF-cx DFT calculations. However, correlation also plays a role, and the mix of exchange and correlation is just as important as the exchange and the correlation by themselves. For this reason, we evaluate PPs with a number of different XC choices.

For small values of s, the $F_x(s)$ of PBEsol [49] follows the cx13 exchange better than PBE, Fig. 4. The small-s behavior of PBEsol exchange motivates us to study PPs based on PBEsol for use with vdW-DF-cx. We also consider the cx13, and we combine it with PBE correlation because of the lack of the option to use vdW-DF-cx correlation. Further, we test creating PPs using the B86bPBE [2,50] XC functional, based on the fact that this combination is sometimes used for slightly more long-ranged systems but keeping within the GGA formulation. It has B86b exchange combined with PBE correlation, and the exchange follows cx13 relatively well for large s. For small s, it deviates from cx13 and behaves more like PBE. The PP we created based on B86bPBE was, however, quickly discarded because already the first hcp bulk calculations showed that the lattice constants are overly large, at 0.5% larger than the hcp bulk results with which we compare.

The PBE enhancement function deviates from cx13 at small s values, while PBEsol follows cx13 better. We therefore expect, from the exchange alone, that PBEsol will be a better choice than PBE in vdW-DF-cx calculations in dense matter. For large s values, both PBE and PBEsol deviate from cx13.

In the end, we carry out extensive tests of four new two-valence electron Mg PPs and their hole companions, as well as the PBE-based PP of Ref. [3], all listed in Table I. To focus the present test on the PP accuracy, and not on general DFT accuracy or XC choice in the DFT calculations, we compare to the results of using 10-valence electron Mg PPs that are obtained from PSLibrary and the GBRV library, and to our Wien2k-based all-electron DFT calculations.

2. Electronic reference configuration

The electron configuration of the atom for the PP is often chosen as the distribution of electrons in the orbitals of an isolated atom, and it requires a division of the electron orbitals into core and valence orbitals. In our project, for Mg with two valence electrons, the core orbitals are $1s^2\ 2s^2\ 2p^6$, and the filled valence orbital is $3s^2$. For PP creation it is generally suggested [25] to include an (empty) state of angular momentum one level higher than that of the core electrons, and use that state as the local reference state for the plane-wave calculations. Our highest angular momentum among the core states is for $2p$, and thus the $3d$ state is a candidate for such reference state. The PP from Ref. [3] follows this suggestion, i.e., it includes the explicitly forbidden $3d$ state (by including "$3d$–1" in the configuration in the PP generation) and uses this state as the local reference state (keyword `lloc = 2`). However, it is also possible to instead pseudize the all-electron potential (keyword `lloc = -1`) and then not include (in our case) an explicitly forbidden $3d$ state in the electronic configuration. In our work, we test both choices.

In our PPs with all-electron pseudization, we also choose to move 25% of an electron from the $3s$ orbital to $3p$, as discussed in the Methods section. This results in the configuration "1s2 2s2 2p6 3s1.75 3p0.25." This choice of configuration follows parts of the literature and is not essential for our results, but it does affect them slightly. For example, our initial results showed that the bulk lattice constants decrease by 0.04% (or 0.11%) when going from 0 to 0.25 (or 0.50) electrons in the $3p$ state (and accordingly 2.00 to 1.75, or 1.50 electrons in the $3s$ state), everything else unchanged.

With the change of electronic configuration and XC choices, several radii in the input to the PP creation may need to be adjusted, not least for the hole versions of the PPs. In practice, the range of values of the radii that will result in usable PPs is rather restricted (and different among the PPs). We found that for the PP to pass the first tests of transferability and of being able to create an identical $2p$-hole version, we often needed the various radii to be slightly smaller than used in Mg-pbe-us-3d.

3. Ultrasoft or PAW

Two of our sets of PBEsol PPs are created identically, except for the choice of US in one (which we name here Mg-pbesol-us) and the PAW approximation in the other (resulting in Mg-pbesol-paw). In each set, the core-hole version is created identically to the nonhole version, except for removing one $2p$ electron in the electronic configuration. This makes it possible to see the effect on bulk and surfaces of including PAW.

In the following subsections, we report and discuss how well these PPs work in the bulk and surface.

B. Mg bulk structure

After testing the PPs for ghost-states and transferability (ions) as single, isolated atoms during the creation of the PPs, the PPs in Mg bulk structures are tested next. While we ultimately need PPs that work well for physisorption and other problems with dominating long-range interactions, it is

TABLE II. Mg bulk lattice constants a and c, formation energies ΔE, Mg(0001) surface energy σ, top layer relaxation $\delta_{12} = (d_{12} - d_{\text{bulk}})/d_{\text{bulk}}$, and surface core level shifts (SCLSs) in the first-layer Mg atoms, relative to bulk signal, calculated with various pseudopotentials (PPs) and in all-electron calculations, using PBE and vdW-DF-cx exchange-correlation functionals. Primitive unit cells are used for all bulk calculations, with k-point samplings $40 \times 40 \times 24$ (hcp) and $44 \times 44 \times 44$ (fcc and bcc), and wave-function (charge-density) energy cutoff $E_{\text{cut}} = 40$ Ry ($E^{\rho}_{\text{cut}} = 320$ Ry) for all PP DFT calculations except those involving the 10-valence electron PPs (Mg-pbe-us-10e-3d, Mg-pbesol-paw-10e-3d, and Mg-pbesol-paw-10e-gbrv) where $E_{\text{cut}} = 120$ Ry ($E^{\rho}_{\text{cut}} = 960$ Ry) is used. For the all-electron calculations, the converged parameters are given in the text. The Mg(0001) surface energies are calculated from 23-layer slabs with all atom positions relaxed, and the SCLS values are from 5×5 surface unit cells. Pseudopotential names are changed and abbreviated here for systematics; full original names are listed in Table I. Data shown here are converged results from Tables S1, S3, and S4 from the Supplemental Material [21].

Pseudopotential	Functional	a_{hcp} (Å)	c (Å)	c/a_{hcp}	a_{bcc} (Å)	a_{fcc} (Å)	$\Delta E_{\text{bcc-hcp}}$ (meV/atom)	$\Delta E_{\text{fcc-hcp}}$ (meV/atom)	σ (meV/Å^2)	δ_{12} (%)	$\Delta_{1,\text{bulk}}$ (meV)
Mg-pbe-us-3d	PBE	3.192	5.188	1.626	3.576	4.519	29	13	34	+1.32	+125
Mg-pbe-us-10e-3d	PBE	3.191	5.187	1.626	3.576	4.518	29	12	34	+1.46	
All-electron (Ref. [41])	PBE	3.193	5.184		3.576	4.522	29	13			
Mg-pbe-us-3d	vdW-DF-cx	3.181	5.169	1.625	3.563	4.503	30	14	43	+1.61	+158
Mg-cx13pbe-paw-3d	vdW-DF-cx	3.192	5.186	1.625	3.575	4.519	30	14	42	+1.55	+151
Mg-pbesol-us	vdW-DF-cx	3.192	5.190	1.626	3.577	4.520	31	14	42	+1.71	+138
Mg-pbesol-paw	vdW-DF-cx	3.199	5.201	1.626	3.584	4.530	31	14	42	+1.73	+139
Mg-pbesol-paw-3d	vdW-DF-cx	3.192	5.186	1.626	3.575	4.519	30	14	43	+1.55	+151
Mg-pbesol-paw-10e-3d	vdW-DF-cx	3.191	5.186	1.625	3.575	4.518	30	14	42	+1.74	
Mg-pbe-us-10e-3d	vdW-DF-cx	3.192	5.187	1.626	3.576	4.518	30	13	42	+1.75	
Mg-pbesol-us-10e-gbrv	vdW-DF-cx	3.194	5.191	1.625	3.578	4.522	30	14	42	+1.65	
All-electron (this work)	vdW-DF-cx	3.193	5.185	1.624	3.575	4.519	30	14			
Experiment[a] at 25 °C		3.20922	5.21067	1.62366							
Experiments									47[b]	1.76[c]	
Experiments									49[d]	1.9 ± 0.3[e]	

[a]Reference [43] (average of six sources).
[b]Reference [51]. Zero-temperature surface energy estimated from melted Mg, that is; from several crystallographic orientations.
[c]Reference [52].
[d]Reference [53]. Zero-temperature surface energy estimated from melted Mg, that is; from several crystallographic orientations.
[e]Reference [54].

imperative that the PP also gives rise to reasonable bulk and surface structures.

To study the convergence of structure and formation energies of the Mg bulk phases hcp, bcc, and fcc, we test a range of values of wave-function energy cutoff (E_{cut}) and k-point samplings, for all the PPs in vdW-DF-cx DFT calculations, and for Mg-pbe-us-3d and Mg-pbe-us-10e-3d also in PBE DFT calculations. We calculate the lattice constants of the hcp, bcc, and fcc phases of Mg, as well as the increase in energy per atom of the bcc and fcc phases compared to the hcp phase.

The convergence results are presented in the Supplemental Material, Table S1 [21]. For the two-electron PPs, we test values $E_{\text{cut}} = 40$, 50, and 60 Ry, with the electron density cutoff energy $E^{\rho}_{\text{cut}} = 8E_{\text{cut}}$; for the 10-electron PPs we test $E_{\text{cut}} = 70$, 90, 100, 110, 120, and 130 Ry, again with $E^{\rho}_{\text{cut}} = 8E_{\text{cut}}$. For hcp Mg we test the k-point samplings $10 \times 10 \times 6$, $20 \times 20 \times 12$, $30 \times 30 \times 18$, $40 \times 40 \times 24$, and $50 \times 50 \times 30$, and for the calculations of bcc and fcc Mg we use the same k-point densities, which for the primitive unit cells of bcc and fcc correspond to the k-point samplings 12, 22, 32, 44, and 54 along each of the three reciprocal-lattice vectors.

We find that at a k-point sampling of $40 \times 40 \times 24$ the hcp phases are structurally very well converged (the bcc and fcc phases are structurally converged already for lower k-point densities), and that a wave-function energy cutoff at 40 Ry (120 Ry) is sufficient when the system only contains Mg atoms with a two-electron (10-electron) PP. This yields high accuracy with the present Mg PPs, in the absence of other atomic species. For the PPs not reported in Table S1 [21], similar tests were carried out, but with E_{cut} and k-point sampling values closer to the values already found sufficient for the other PPs. Results of lattice constants and formation energy differences for the chosen k-point sampling and energy cutoffs are extracted and presented for all PPs in Table II.

In Table II we include values from experiment for the Mg hcp lattice constants at 25 °C, because no low-temperature results are available. We also include values from our all-electron calculations for hcp, fcc, and bcc lattices with vdW-DF-cx DFT, and all-electron results from the literature [41] carried out with PBE PPs using the PBE functional in the DFT calculations.

For PBE DFT calculations (top part of Table II) we find that the converged two-electron PP results (Mg-pbe-us-3d) yield lattice constants in agreement both with results from the 10-electron PP and the all-electron calculations. This also applies to the difference in formation energies, $\Delta E_{\text{bcc-hcp}}$ and $\Delta E_{\text{fcc-hcp}}$. In other words, in this system of bulk Mg where

the PBE XC approximation is sufficient (no dispersion), the two-electron PP of Ref. [3] works well.

Evaluating then the five two-electron PP sets in vdW-DF-cx calculations (PPs Mg-pbe-us-3d through Mg-pbesol-paw-3d in Table II) it becomes clear that the Mg-pbe-us-3d PP, which worked well with PBE, yields lattice constants in all phases that are too small by about 0.01 Å, even when compared to the similar 10-electron PP Mg-pbe-us-10e-3d. This indicates that this PP should not be used with vdW-DF-cx, and that we must indeed create and use other PPs for vdW-DF-cx calculations when two-electron PPs are needed.

Of the other four PPs, the Mg-pbesol-paw performs the worst. Although not all its lattice constants deviate as much from the 10-electron and all-electron results as the Mg-pbe-us-3d, the lattice constants are systematically too large, and given that better PPs (from this aspect) are available, the Mg-pbesol-paw should probably not be used.

All three other two-electron PPs have good or very good lattice constants, compared to the 10-electron and all-electron results. We also note that the three 10-electron PPs used here all give very similar results even though they have been created with vastly different parameters and different codes.

Turning to the formation energies $\Delta E_{\text{bcc-hcp}}$ and $\Delta E_{\text{fcc-hcp}}$, we see that they are the same for all PPs (and the all-electron calculations) within the same XC choice in the DFT calculations, and they are almost the same for PBE and vdW-DF-cx calculations. The formation energy is not sensitive to the choice of PP nor the choice of XC in DFT (within the choices reported here).

Finally, we also report results from experiment. We find that our values of the lattice constants for hcp (the only lattice constants available from experiment) are smaller than the room-temperature measurements, which is not surprising.

C. Mg(0001) structure

Moving on to the surface calculations, we focus on the energetically most favored [3,4] crystallographic orientation, Mg(0001). The traditional way to describe a surface in a DFT calculation with periodic boundary conditions is to model the surface with a slab of material and a sufficient amount of vacuum in order to minimize unwanted interactions between periodic copies of the slab. Often the slabs are chosen rather thin, with just a few atomic layers. However, Ref. [39] found that for certain physical properties, such as the interlayer distances further down into the bulk, the size of the slab needed for converged distances (the "Thin-film limit") is 23 atomic layers (∼60 Å), while properties such as the surface energy and top interlayer distance are converged with a smaller (but still not very thin) slab. Reference [39] defines the thin-film limit as the thickness at which the interlayer relaxation in the middle of the slab is less than ±0.10%.

While testing the values of the relaxations obtained with our various PPs and making sure the calculations represent the surface properly, we also test the number of atomic layers needed for such convergence. Tables S2 and S3 of the Supplemental Material [21] contain the layer relaxations for a 19-layer slab (Table S2) and a 23-layer slab (Table S3). Calculations for four of the two-electron PP and DFT combinations, for the top and middle interlayer distances, are summarized in Table III. A fast comparison shows that, indeed, the interlayer distances inside the slab, d_{mid}, are not converged with a 19-layer slab. In the middle of the slab, the distances are relatively far from the bulk distance $d_{\text{bulk}} = c/2$ (at 0.12–0.17% larger). For the 23-layer slab, the middle of the slab is closer to the bulk structure (0.04–0.08% smaller, when including all results from Table S3 [21]). We note that these offsets for the middle of the 23-layer slab also apply to the 10-valence electron PPs; whether the $2p$ electrons are included as valence electrons or not has no effect (suggested in Ref. [39]). While we could have tested even more layers in the slab, we decided that for our work a 23-layer slab is sufficiently converged for bulk properties, as also found in Ref. [39].

For surface properties, such as the surface energy σ and the top interlayer distance d_{12}, and its deviation from the bulk value $\delta_{12} = (d_{12} - d_{\text{bulk}})/d_{\text{bulk}}$, Ref. [39] finds 18 layers (or even fewer) to be sufficient. We find that d_{12} is not converged for 19 layers, with a larger deviation from d_{bulk} in 19 layers than in 23 layers (Table III, as well as Tables S2 and S3 [21]). While we do not test still larger slab thickness, we assume the 23 layers to be sufficient for our purposes, given also that at least the vdW-DF-cx DFT calculations give results close to experiment.

For each choice of XC and PP, the surface energies σ are the same for 19 and 23 layers, within the accuracy of the DFT calculations, and they are therefore converged with respect to the number of layers already at 19 layers. The σ is given in Tables S2 and S3 [21] but also summarized in Table II for all PPs and DFT combinations studied.

We note that within each choice of XC (PBE or vdW-DF-cx) for DFT there is no difference in values of σ regardless of the choice of PP. We do, however, see a significant difference with the choice of XC in DFT calculations. PBE DFT calculations yield smaller σ values ($\sim$34 meV/Å^2) than the vdW-DF-cx DFT calculations ($\sim$42 meV/Å^2) almost independently of the choice of PP and whether the PP has 2 or 10 valence electrons. We find that vdW-DF-cx surface energies are 25% larger than the PBE surface energies and closer to the experimental values. Experimental values for the surface energy are estimated from the surface tension of the liquid-vapor interface at the melting point of Mg, extrapolated to zero temperature, at 49 meV/Å^2 (Ref. [51]) and 47 meV/Å^2 (Ref. [53]); being a melt, this includes a mixture of surface orientations, not only the lowest-energy Mg(0001) surface, so the numbers should be seen as an upper estimate of the Mg(0001) surface energy. We are unable to find the experimental result cited in Ref. [39] of 0.28 eV/atom ($\approx$32 meV/Å^2): the citation in Ref. [39] pertains to work that does not report any surface energies, and we find no such result anywhere else in the literature.

We therefore believe that our vdW-DF-cx results, that are closer in value to the $47 - 49$ meV/Å^2 experimental results actually found in the literature, yield a better representation of the surface than PBE results. This is not surprising because vdW-DF-cx in general is expected to represent surfaces better than PBE. It has been shown [17] that for a broad range of surfaces, vdW-DF-cx gives better surface energies and work functions than, for example, PBE. The work function quality is directly related to the quality of the electron density, via

TABLE III. Relaxations of layer distances d_{ij} in the top and middle of a 19- and 23-layer Mg(0001) slab, and the distance relative to the bulk distance $\delta_{ij} = (d_{ij} - d_{\text{bulk}})/d_{\text{bulk}}$.

	Mg-pbe-us-3d, PBE	Mg-pbe-us-3d, vdW-DF-cx	Mg-pbesol-us, vdW-DF-cx	Mg-pbesol-paw, vdW-DF-cx
d_{bulk} (Å)	2.594	2.585	2.595	2.600
		19 layers		
d_{12} (Å)	2.631	2.630	2.642	2.647
δ_{12} (%)	+1.43	+1.75	+1.82	+1.80
d_{mid} (Å)	2.597	2.588	2.599	2.605
δ_{mid} (%)	+0.12	+0.12	+0.17	+0.17
		23 layers		
d_{12} (Å)	2.629	2.626	2.639	2.645
δ_{12} (%)	+1.32	+1.61	+1.71	+1.73
d_{mid} (Å)	2.592	2.583	2.594	2.599
δ_{mid} (%)	–0.08	–0.05	–0.05	–0.05

the Poisson equation, and therefore motivates that the electron density in the vicinity of surfaces is better described with vdW-DF-cx. This, in turn, is expected to lead to better descriptions of surface properties such as the surface energy, but also the surface layer relaxations. These results are also in nice agreement with a similar DFT study by Kebede *et al.* [10] in which the surface energy of MgO(001) was calculated for a series of XC choices, using the DFT code VASP [55], and found to be up to 50% larger for vdW-aware XC calculations than for PBE calculations (27% for vdW-DF-cx relative to PBE), and closer to experimental results.

The better electron density description is also reflected in the fact that the change in interlayer distance δ_{12} in the top layer for vdW-DF-cx here gives results ($\delta_{12} = +1.55\%$ to $+1.75\%$, Table II) that are close to the experimental results ($\delta_{12} = 1.76\%$ to $1.9 \pm 0.3\%$), while for DFT calculations with PBE the δ_{12} is smaller. In other words, the surface is sensitive to the inclusion of dispersion interactions in the DFT calculations, both for structure (δ_{12}) and energy (σ).

Regarding the quality of the PPs, the main focus of this paper, none of the PPs tested here yield surface calculations that stand out as poor, and judging solely from the 23-layer slab calculations, while some PPs are better than others, they are all usable. The choice of XC in the DFT calculations is more important for the various surface properties than the choice of PP.

D. SCLS in clean Mg(0001)

The main reason we create two-valence electron PPs is to use them in SCLS calculations. We test the PPs and their hole companions by calculating the SCLS in the top five atomic layers of clean Mg(0001). In the DFT calculations, the hole-containing Mg atoms must be well separated to not interact. Because the DFT calculations use periodic boundary conditions, we need side lengths of the surface unit cells of ~16 Å, which we obtain with 5×5 surface supercells. For a 23-layer slab, this requires 575 Mg atoms per calculational unit cell—this is not impossible, but for further work with more involved systems it is worth trying to find ways to bring the computational burden down, without loss of accuracy.

Since much of the interaction happens on or in the first few atomic layers of the surface, we test whether we may "shave" off the bottom of the slab, keeping the remaining atomic layers in their original 23-layer slab positions. We decide to keep the nine top layers (and in interactions with the surface, for example adsorption of O atoms, letting the top four atomic layers further relax their positions—however, this is not relevant in the work presented here).

By calculating the SCLSs of the full and truncated surfaces, Tables IV and S4 [21] (columns marked Top-9 and All), we can compare the SCLS values (1) from the two surface models. We find that for the top layer SCLS, $\Delta_{1,\text{bulk}}$, the difference using the Top-9 layers compared to the full slab is either vanishingly small (for PBE) or just a couple of meV (for vdW-DF-cx). For the $\Delta_{i,\text{bulk}}$ values in lower layers, where the SCLS in itself is small, the deviations are larger, up to 11 meV, but still reasonable, given that the XPS measurements that will be compared to often have accuracy of the same size, or even worse.

While the calculations of SCLS in the 23-layer slab are symmetric around the center plane (one hole in each end of the surface), the Top-9 slab has only one hole, and the slab itself is also slightly asymmetric. If this creates an artificial dipole across the slab, the periodic images will interact because dipoles interact on long ranges, even across 15 Å of vacuum. This can be handled by a dipole correction [56] in Quantum Espresso. We check whether the dipole correction is needed by calculating two of the SCLS values in one of the surfaces with the dipole correction (Tables IV and S4 [21]). Comparing the Top-9 values with the Top-9^{dip} we find that there is no difference, and we therefore do not use the dipole correction in further calculations.

Studying the top layer SCLS results, $\Delta_{1,\text{bulk}}$ of Table S4 [21], and also presented in Table II, we note that DFT calculations with PBE generally give rise to smaller SCLS values than calculations with vdW-DF-cx. This may be the indirect result of the general difference in surface layer relaxation, discussed in the previous subsection. While for DFT with

TABLE IV. Surface core level shifts $\Delta_{i,\mathrm{bulk}}$ relative to bulk in a 23-layer Mg(0001) slab. Results for slabs containing only the top nine atomic layers of a 23-layer slab while keeping the positions of the four lowest layers in their original positions, without (Top-9) or with (Top-9$^{\mathrm{dip}}$) dipole correction, and for slabs containing all 23 layers (All), in that case using one core hole on each side of the slab in symmetric positions. Shown are results for two representative choices of pseudopotentials and exchange-correlation. The size of the surface unit cell is 5×5, with $8 \times 8 \times 1k$-points. The wave-function (charge-density) energy cutoff is $E_{\mathrm{cut}} = 40$ Ry ($E^{\rho}_{\mathrm{cut}} = 320$ Ry). Values in meV. Further results are presented in Table II for $\Delta_{1,\mathrm{bulk}}$ and in Table S4 [21] for other shifts.

	Mg-pbe-us-3d			Mg-pbesol-paw	
	with PBE			with vdW-DF-cx	
	Top-9	Top-9$^{\mathrm{dip}}$	All	Top-9	All
$\Delta_{1,\mathrm{bulk}}$ (meV)	+125	+125	+125	+143	+139
$\Delta_{2,\mathrm{bulk}}$ (meV)	−7	−7	−13	−5	−16
$\Delta_{3,\mathrm{bulk}}$ (meV)	−8	−8	−10	−9	−14

PBE we find the values of $\Delta_{1,\mathrm{bulk}} = 125$ meV, the vdW-DF-cx calculations give values in the range 138–158 meV, where PPs with the $3d$ orbital used for the local potential give the largest SCLS values (151–158 meV). These are all energies relative to those of a hole in a Mg atom placed deep into bulk, which is not the situation in XPS measurements where the "bulk" signals come from lower-lying layers, not fully into bulk, but for comparison of methods it is useful to compare values to a hypothetical, independent "real" bulk value. How we correct these values to obtain quantities that better reflect the XPS-obtained "bulk" signal is described in Sec. IV E.

Similar to the surface calculations, we can conclude for the SCLS calculations presented here that we cannot rule out any of the PPs as unreasonable, but that the differences between them are not negligible. We find larger SCLS values $\Delta_{1,\mathrm{bulk}}$ in vdW-DF-cx DFT calculations than in PBE DFT calculations.

E. Bulk peaks in XPS spectra

In fitting experimentally obtained XPS spectra to SCLS values from theory, it is imperative to note that what comes out as "bulk" signals in experiments are a weighted sum of contributions from atoms in layers slightly lower than the atoms on top of the surface. The bulk atoms deep into the surface do not contribute to the signal [4]. The measured "bulk" peak may thus be shifted a bit from the position of a hypothetical, real bulk signal, and this becomes important for spectra with high resolution and several features present within a small range of energies [4].

For Mg(0001) we see from Tables IV and S4 [21] that the top atoms are expected from theory to give rise to a signal at 0.1–0.2 eV from the other, lower atoms. To estimate the peak position for these lower atoms (relative to real bulk), we assume that each of the layers 2–4 contributes with an intensity proportional to $\exp(-\delta/\lambda)$, where δ is the atom's distance from the top layer, and $\lambda \approx 5.6$ Å is the escape depth in Mg for photon energies [57] around 100 eV. For this estimate, we use a superposition of Gaussian distributions with standard deviation 50 meV for each of the three contributions (layers 2–4), and we calculate the position of its maximum. This results in an expected "bulk" peak for Mg(0001) with maximum at position −5 meV (−11 meV) relative to a hypothetical signal from real bulk in PBE with the Mg-pbe-us-3d PP (in vdW-DF-cx with the Mg-pbesol-paw-3d PP) calculations. The result is not sensitive to reasonable variations in the value of λ, nor to the chosen value of the Gaussian standard deviation used for this estimate.

F. MgO phases

Our final test of the PPs in environments dominated by short-range interactions is the structure of three MgO bulk phases: The RS, WZ, and h-MgO phases, Fig. 3.

In Table S5 [21] for the RS phase we present a convergence study of k-point sampling and kinetic energy cutoff values E_{cut}. In general, metals need a more dense k-point sampling than their oxides, and we expect to need fewer k-points for MgO than for the Mg hcp (and bcc, fcc) phase. The Mg hcp converged k-point sampling $40 \times 40 \times 24$ is the same density as in a $46 \times 46 \times 46$ RS primitive unit cell, given the approximate lattice constants $a_{\mathrm{hcp}} = 3.2$ Å, $c_{\mathrm{hcp}} = 5.2$ Å, and $a_{\mathrm{MgO}} = 4.2$ Å. For two of the PPs (one two-valence electron and one 10-valence electron) we therefore test a series of less dense samplings $n_k \times n_k \times n_k$ with $n_k = 36$, 30, 26, 20, 16, 10, 6, and 4, Table S5 [21]. Convergence in k-points is achieved at $10 \times 10 \times 10k$-points, and other PPs are tested only with $n_k = 26$ and smaller. We find that even fewer k-points than $n_k = 10$ would be reasonable choices, but for now we keep the $n_k = 10$ in further calculations. This applies to all of the PPs, and also PPs for which the convergence tests are not explicitly shown in Table S5 [21].

Regarding the energy cutoff, we find that in RS bulk with two-electron PPs, 100 Ry is necessary for convergence, mainly because the O atom PPs require high values of E_{cut}. For the 10-electron PPs, already the Mg PPs need a 120 Ry cutoff, setting the requirement from the Mg PPs higher than from the O PPs.

In Table S5 [21] we only show the results of five sets of calculations; our other combinations of PPs and DFT XC choice have the same need for k-points and cutoff energy for convergence, and they are all summarized for the converged parameters in Table V. For the same five sets we also check the k-point convergence of the WZ and h-MgO phases, with results shown in Table S6 [21], as well as their formation

TABLE V. MgO bulk lattice constants a and c (in Å) and internal parameter u, as well as difference in formation energies (in meV/formula unit), for rocksalt (RS), wurtzite (WZ), and hexagonal-MgO (h-MgO) phases. Converged k-point samplings for primitive unit cells $10 \times 10 \times 10$ for RS and $8 \times 8 \times 6$ for WZ and h-MgO. Converged kinetic energy cutoff E_{cut} in Ry, and charge density cutoff used is $8E_{\text{cut}}$. Results from pseudopotential calculations with Quantum Espresso, except the all-electron results that are from Wien2k-calculations, converged as described in the main text.

	E_{cut}	a_{rs}	a_{wz}	c_{wz}	u_{wz}	a_{h}	c_{h}	$\Delta E_{\text{wz-rs}}$	$\Delta E_{\text{h-rs}}$
DFT with PBE:									
Mg-pbe-us-3d & O-pbe-us	100	4.249	3.311	5.115	0.3919	3.517	4.233	140	72
Mg-pbe-us-10e-3d & O-pbe-us	120	4.253	3.314	5.119	0.3920	3.520	4.238	139	72
All-electron (this work)		4.255				3.522	4.239		72
All-electron[a] (Ref. [42])		4.259							
DFT with vdW-DF-cx:									
Mg-pbe-us-3d & O-pbe-us	100	4.222	3.311	5.030	0.3974	3.498	4.212	261	160
Mg-cx13pbe-paw-3d & O-pbesol-paw	100	4.224	3.312	5.034	0.3974	3.500	4.212	258	157
Mg-pbesol-us & O-pbesol-paw	100	4.249	3.332	5.067	0.3971	3.521	4.240	262	161
Mg-pbesol-paw & O-pbesol-paw	100	4.255	3.338	5.068	0.3977	3.526	4.245	267	163
Mg-pbesol-paw-3d & O-pbesol-paw	100	4.230	3.320	5.029	0.3984	3.505	4.218	268	164
Mg-pbesol-paw-10e-3d & O-pbesol-paw	120	4.227	3.314	5.034	0.3975	3.501	4.218	250	153
Mg-pbe-us-10e-3d & O-pbe-us	120	4.230	3.316	5.036	0.3975	3.503	4.220	249	152
Mg-pbesol-us-10e-gbrv & O-pbesol-us-gbrv	120	4.228	3.314	5.034	0.3975	3.502	4.219	249	152
PAW, eight-electron Mg pseudopot.[b] (Ref. [10])	29	4.22							
All-electron (this work)		4.226				3.499	4.217		154
All-electron[a] (Ref. [42])		4.231							
Experiment at 19.8 K (Ref. [44])		4.207							
Experiment - ZPAE[c] 0 K (Ref. [45])		4.18							
Fitted experiment[d] (Ref. [58])			3.283	5.095	0.388				

[a]Wien2k all-electron calculations. The vdW-DF-cx results are from non-self-consistent calculations using a PBE charge density.
[b]VASP vdW-DF-cx PAW calculations using Mg pseudopotentials with eight valence electrons, k-point sampling $4 \times 4 \times 4$.
[c]Subtracted temperature contributions using the zero-point anharmonic expansion (ZPAE).
[d]From fits to $Mg_xZn_{1-x}O$ experimental data.

energy differences. Again, we find the k-point density equivalent to RS $10 \times 10 \times 10k$-points (approximately $8 \times 8 \times 6$ for the WZ and h-MgO phases) to be well converged, and if needed a decrease to $6 \times 6 \times 6$ / $6 \times 6 \times 4$ would be acceptable. These numbers, for the converged WZ and h-MgO phases, are also summarized in Table V, along with the results from our other PPs in this study.

Comparing the lattice constants in Table V, we find that in the PBE DFT calculations, the two-electron Mg PP yields slightly too small lattice constants, compared to the results from the 10-electron Mg PP (in the two sets of calculations, the same O PP is used), and also compared to the all-electron PBE calculations.

In the vdW-DF-cx DFT calculations, the lattice constant values obtained with two of the Mg PPs stand out with values that are too large by $\sim 0.02 - 0.03$ Å in all three MgO phases, compared to the 10-electron and all-electron vdW-DF-cx calculations: the Mg-pbesol-us and the Mg-pbesol-paw. Choosing here a PP with the local potential pseudized in the $3d$ state seems to be important for results of two-electron PPs but not for 10-electron PPs. We note that the MgO calculations with the less good results have been calculated with the same O PP as the results of the two better-performing Mg PPs—the Mg-cx13pbe-paw-3d and Mg-pbesol-paw-3d—so the choice of O PP has no effect on this conclusion of Mg PP quality.

Between the PBE and vdW-DF-cx DFT calculations, we see that the MgO lattice constants in general are smaller for the latter. This agrees well with findings in Ref. [10] that vdW-DF-cx is among the three dispersion-aware XC choices they tested that show the best overall performance for bulk MgO and NaCl, and with the expectation that long-range interactions in vdW-DF-cx will give stronger bonding in the oxides than for PBE.

Within the vdW-DF-cx calculations, the formation energy differences $\Delta E_{\text{wz-rs}}$ and $\Delta E_{\text{h-rs}}$ hardly vary with the choice of the two-electron PP. The values are slightly smaller for the 10-electron PPs and the all-electron calculations, but the large difference is in the formation energies of PBE DFT and vdW-DF-cx DFT calculations: going from the RS phase to the WZ phase (RS to h-MgO) costs 140 meV/formula unit (72 meV/formula unit) in PBE, but approximately double that in vdW-DF-cx calculations, at a cost of 265 meV/formula unit (163 meV/formula unit).

In Table V we also include lattice constants for the RS and WZ phases from experiments. In the RS phase, the experimental lattice constants are smaller than in our calculations, but with vdW-DF-cx results a bit closer to experiment. For the WZ phase, the experimental values are extrapolated values, and they are close to our results.

G. What can we recommend?

We set out to create PPs to be used with the vdW-DF-cx DFT calculations, and to test an existing PP in PBE

calculations. The results obtained can help us find which PP to use, if it has already been determined which of PBE and vdW-DF-cx will be used in the DFT calculations, but the results can also help us recommend whether or not PBE is sufficiently accurate for use in the DFT calculations.

With the test results described and discussed here, we find that for *PBE DFT calculations*, the Mg-pbe-us-3d PP of Ref. [3], and also used by us in Ref. [4], works very well. Compared to the use of a similar 10-electron PP, the Mg lattice constants, formation energies, and surface energies are as well described with the two-electron PP. There is a small difference in interlayer relaxation in the top layer of the Mg(0001) surface, and the oxide lattice constants also deviate somewhat (0.003–0.004 Å) from the results with the 10-electron PP and all-electron calculations, while the formation energy differences between the RS, WZ, and *h*-MgO phases are not affected by the fewer electrons. In other words, if the DFT calculations must be carried out with PBE, then the Mg-pbe-us-3d PP is a good choice.

If *vdW-DF-cx is the choice used for the DFT calculations*, not all five tested two-electron PPs work equally well. First of all, while Mg-pbe-us-3d is good for use with PBE, it fails some of the tests with vdW-DF-cx. Already the lattice constants for bulk Mg are not well-described by this PP, compared to 10-electron PPs and all-electron calculations. The lattice constants are too small. This PP works better in MgO, but we want a PP that can be used both with and without oxide patches in the material, and we therefore discard the PP Mg-pbe-us-3d.

Of the four other tested two-electron PPs, the Mg-pbesol-paw consistently gives lattice constants for the Mg bulk phases that are too large, compared with 10-electron PPs and all-electron calculations. It also overestimates the lattice constants in the MgO bulk phases. The Mg-pbesol-us fares well in the Mg bulk phases, but also overestimes the lattice constants in the MgO bulk phases. We therefore also discard the PPs Mg-pbesol-paw and Mg-pbesol-us for use with vdW-DF-cx DFT calculations.

The two remaining PPs—the Mg-cx13pbe-paw-3d and Mg-pbesol-paw-3d—both work well with the Mg bulk phases, with almost identical results, and while there is more spread on their results for the MgO bulk phases, the differences are not enough to value one over the other. For vdW-DF-cx DFT calculations, we therefore recommend either Mg-cx13pbe-paw-3d or Mg-pbesol-paw-3d. Further distinction can be discovered by us or other researchers using these PPs for specific tasks.

As we have seen, in many quantities the choice of XC in the DFT calculations affects the results more than the choice of PP. It affects surface energies, surface relaxations, and SCLS, as well as formation energies of the MgO phases. With the results presented here, we can make recommendations also on the DFT XC choice (between PBE and vdW-DF-cx).

We find that for the Mg surface structure and surface energy, in the oxide bulk, and for the SCLS values, it matters whether dispersion interactions are discarded (in PBE) or kept (in vdW-DF-cx), while the Mg bulk phases are not affected. As discussed in previous sections, where differences are shown between PBE and vdW-DF-cx DFT calculations and where the results can be compared to experiments, the differences are in favor of vdW-DF-cx. As was shown in Ref. [17] for a range of surfaces, the vdW-DF-cx gives better surface energies and work functions, which, in turn, implies better electron densities close to the surface. The same applies for ionic crystals, where dispersion interactions are crucial [5–10]. Our results fit nicely with these expectations, and show that in most of the cases treated here, the dispersion interactions should not be ignored, and of PBE and vdW-DF-cx, the latter should be selected.

Finally, we would like to address the fact that this study is focused on a specific material and signal in XPS measurements, namely the $2p$ signal from Mg. The way we have decided on how to create the PPs and how we have tested them is, however, more general. Modern PPs often include both valence electrons and what might be called semicore electrons in the "valence" portion of the PP. This is because the description is often better with more valence electrons, and while it comes at a higher computational cost (e.g., the 10-electron Mg PPs require 120 Ry energy cutoff, while 40 Ry suffices for the two-electron PPs), in many cases this is not an important limit any longer. Thus, there are many nice and well-tested PPs around, but often they include the semicore states among the valence electrons. If such a state is of interest in XPS measurements, it can therefore be hard to find a PP with that state put into the PP core states, not the valence states, in order to create an accompanying hole PP. This could be, for example, the Ca $3p$ or $3s$ signal, the K $3s$ signal, or possibly some of the transition metals, although these may create other problems when restricting to a smaller set of valence electrons in the PP.

V. SUMMARY

We have described and discussed the creation of two-electron Mg PPs for use in SCLS calculations, but also for calculating other properties of Mg surfaces. We have carried out extensive convergence studies of both Mg and MgO bulk phases. In our study, we include three standard 10-electron Mg PPs for comparison, both from PSLibrary (created with `ld1.x`) and the GBRV library. Where needed, we calculate all-electron results for the Mg and MgO bulk phases. We evaluate SCLSs in the Mg(0001) surface and observe a difference in choice of XC for the DFT calculations, where the SCLSs are larger when dispersion is included. The differences between choices of PPs are less pronounced, and we also find that our strategy of shaving off the top nine layers of a 23-layer Mg(0001) slab, to use for SCLS calculations, works well. We estimate where in an XPS spectrum to expect the bulklike signal to appear, compared to the hypothetical signal that would arrive from far down into the bulk; those are the values obtained by and compared in theory. We see the difference in PBE and vdW-DF-cx XC choices in DFT calculations. While this was not the main goal of this work, our observations can aid decisions on which XC to use in DFT calculations of future Mg-based work, and we find that the dispersion-inclusive vdW-DF-cx gives better surface and oxide results, as expected from earlier work. In summary, we found that two of our new Mg PPs are good candidates for further studies of Mg surfaces, oxidation, corrosion, and adsorption in combination with XPS measurements, the Mg-cx13pbe-paw-3d,

and the Mg-pbesol-paw-3d, with the use of vdW-DF-cx DFT. We find that the Mg PP of Ref. [3] works well in PBE DFT calculations such as the calculations of our previous work in Ref. [4], but when better DFT descriptions are needed, this PP works less well in vdW-DF-cx DFT calculations, in particular in the metallic Mg. We expect that our systematic approach to creating and testing the PPs can also be used for other metals where XPS signals come from states that are between core and valence states and often treated as valence states by existing PPs.

ACKNOWLEDGMENTS

We thank Layla Martin-Samos (CNR-IOM/Democritos National Simulation Center, Istituto Officina dei Materiali, Italy) and Miha Gunde (Division of Theoretical Physics, Ruđer Bošković Institute, Croatia) for providing access to the PBE two-valence-electron Mg pseudopotential and its hole companion, created for and used in Ref. [3]. The present work is supported by the Swedish Research Council (VR) through Grant No. 2020-04997, the Swedish Foundation for Strategic research (SSF) through Grant No. IMF17-0324, the Slovenian Research and Innovation Agency ARIS (Research Project No. J2-7157), Chalmers Excellence Initiative Nano, and financial support from China Scholarship Council (No. 201906070278). The computations were performed using computational and storage resources at Chalmers Centre for Computational Science and Engineering (C3SE), and with computer and storage allocations from the Swedish National Infrastructure for Computing (SNIC), now National Academic Infrastructure for Supercomputing in Sweden (NAISS), under Contracts No. SNIC2022/5-388, No. SNIC2022/3-16, No. SNIC2022/6-286, No. NAISS2023/5-356, No. NAISS2023/3-22, No. NAISS2023/6-306, and No. NAISS2024/5-411.

[1] S. García-Gil, A. García, and P. Ordejón, Calculation of core level shifts within DFT using pseudopotentials and localized basis sets, Eur. Phys. J. B **85**, 239 (2012).

[2] J. P. Perdew, K. Burke, and M. Ernzerhof, Generalized gradient approximation made simple, Phys. Rev. Lett. **77**, 3865 (1996).

[3] M. Gunde, L. Martin-Samos, S. de Gironcoli, M. Fanetti, D. Orlov, and M. Valant, First-principles characterization of Mg low-index surfaces: Structure, reconstructions, and surface core-level shifts, Phys. Rev. B **100**, 075405 (2019).

[4] Z. Xing, M. Fanetti, S. Gardonio, E. Schröder, and D. Orlov, Initial oxidation of low index Mg surfaces investigated by SCLS and DFT, Appl. Surf. Sci. **671**, 160656 (2024).

[5] J. Klimeš, D. R. Bowler, and A. Michaelides, van der Waals density functionals applied to solids, Phys. Rev. B **83**, 195131 (2011).

[6] G.-X. Zhang, A. Tkatchenko, J. Paier, H. Appel, and M. Scheffler, van der Waals interactions in ionic and semiconductor solids, Phys. Rev. Lett. **107**, 245501 (2011).

[7] T. Bučko, S. Lebègue, J. Hafner, and J. G. Ángyán, Tkatchenko-Scheffler van der Waals correction method with and without self-consistent screening applied to solids, Phys. Rev. B **87**, 064110 (2013).

[8] E. J. Granhed, G. Wahnström, and P. Hyldgaard, $BaZrO_3$ stability under pressure: The role of nonlocal exchange and correlation, Phys. Rev. B **101**, 224105 (2020).

[9] A. Perrichon, E. Jedvik Granhed, G. Romanelli, A. Piovano, A. Lindman, P. Hyldgaard, G. Wahnström, and M. Karlsson, Unraveling the ground-state structure of $BaZrO_3$ by neutron scattering experiments and first-principles calculations, Chem. Mater. **32**, 2824 (2020).

[10] G. G. Kebede, D. Spångberg, P. D. Mitev, P. Broqvist, and K. Hermansson, Comparing van der Waals DFT methods for water on NaCl(001) and MgO(001), J. Chem. Phys. **146**, 064703 (2017).

[11] M. Dion, H. Rydberg, E. Schröder, D. C. Langreth, and B. I. Lundqvist, van der Waals density functional for general geometries, Phys. Rev. Lett. **92**, 246401 (2004).

[12] K. Berland and P. Hyldgaard, Exchange functional that tests the robustness of the plasmon description of the van der Waals density functional, Phys. Rev. B **89**, 035412 (2014).

[13] T. Thonhauser, V. R. Cooper, S. Li, A. Puzder, P. Hyldgaard, and D. C. Langreth, van der Waals density functional: Self-consistent potential and the nature of the van der Waals bond, Phys. Rev. B **76**, 125112 (2007).

[14] K. Berland, C. A. Arter, V. R. Cooper, K. Lee, B. I. Lundqvist, E. Schröder, T. Thonhauser, and P. Hyldgaard, van der Waals density functionals built upon the electron-gas tradition: Facing the challenge of competing interactions, J. Chem. Phys. **140**, 18A539 (2014).

[15] K. Berland, V. R. Cooper, K. Lee, E. Schröder, T. Thonhauser, P. Hyldgaard, and B. I. Lundqvist, van der Waals forces in density functional theory: A review of the vdW-DF method, Rep. Prog. Phys. **78**, 066501 (2015).

[16] Ø. Borck and E. Schröder, Methylbenzenes on graphene, Surf. Sci. **664**, 162 (2017).

[17] P. Hyldgaard, Y. Jiao, and V. Shukla, Screening nature of the van der Waals density functional method: A review and analysis of the many-body physics foundation, J. Phys.: Condens. Matter **32**, 393001 (2020).

[18] Quantum ESPRESSO, manifesto (2022), https://www.quantum-espresso.org/manifesto/.

[19] P. Giannozzi, S. Baroni, N. Bonini, M. Calandra, R. Car, C. Cavazzoni, D. Ceresoli, G. L. Chiarotti, M. Cococcioni, I. Dabo, A. D. Corso, S. Fabris, G. Fratesi, S. de Gironcoli, R. Gebauer, U. Gerstmann, C. Gougoussis, A. Kokalj, M. Lazzeri, L. Martin-Samos *et al.*, QUANTUM ESPRESSO: A modular and open-source software project for quantum simulation of materials, J. Phys.: Condens. Matter **21**, 395502 (2009).

[20] P. Giannozzi, O. Andreussi, T. Brumme, O. Bunau, M. B. Nardelli, M. Calandra, R. Car, C. Cavazzoni, D. Ceresoli, M. Cococcioni, N. Colonna, I. Carnimeo, A. D. Corso, S. de Gironcoli, P. Delugas, R. A. DiStasio, A. Ferretti, A. Floris, G. Fratesi, G. Fugallo *et al.*, Advanced capabilities for materials modelling with QUANTUM ESPRESSO, J. Phys.: Condens. Matter **29**, 465901 (2017).

[21] See Supplemental Material at http://link.aps.org/supplemental/10.1103/PhysRevMaterials.8.123801 for tables of convergence studies for bulk, surface and surface core level shift properties.

[22] E. Schröder, Interaction effects in magnesium oxidation: A lattice-gas simulation, Comput. Mater. Sci. **24**, 105 (2002).

[23] E. Schröder, R. Fasel, and A. Kiejna, O adsorption and incipient oxidation of the Mg(0001) surface, Phys. Rev. B **69**, 115431 (2004).

[24] K. Garrity, J. Bennett, K. Rabe, and D. Vanderbilt, Pseudopotentials for high-throughput DFT calculations, Comput. Mater. Sci. **81**, 446 (2014).

[25] A. Dal Corso, Pseudopotentials periodic table: From H to Pu, Comput. Mater. Sci. **95**, 337 (2014).

[26] Pslibrary, A library of ultrasoft and PAW pseudopotentials, https://dalcorso.github.io/pslibrary/.

[27] E. Schröder, V. R. Cooper, K. Berland, B. I. Lundqvist, P. Hyldgaard, and T. Thonhauser, Chapter 8 - The vdW-DF Family of Nonlocal Exchange-Correlation Functionals, in *Non-Covalent Interactions in Quantum Chemistry and Physics*, edited by A. Otero de la Roza and G. A. DiLabio (Elsevier, Amsterdam, 2017), pp. 241–274.

[28] D. Vanderbilt, Soft self-consistent pseudopotentials in a generalized eigenvalue formalism, Phys. Rev. B **41**, 7892 (1990).

[29] P. E. Blöchl, Projector augmented-wave method, Phys. Rev. B **50**, 17953 (1994).

[30] S. G. Louie, S. Froyen, and M. L. Cohen, Nonlinear ionic pseudopotentials in spin-density-functional calculations, Phys. Rev. B **26**, 1738 (1982).

[31] N. Troullier and J. L. Martins, Efficient pseudopotentials for plane-wave calculations, Phys. Rev. B **43**, 1993 (1991).

[32] E. Schröder, R. Fasel, and A. Kiejna, Mg(0001) surface oxidation: A two-dimensional oxide phase, Phys. Rev. B **69**, 193405 (2004).

[33] H. J. Monkhorst and J. D. Pack, Special points for Brillouin-zone integrations, Phys. Rev. B **13**, 5188 (1976).

[34] C. G. Broyden, The convergence of a class of double-rank minimization algorithms 1. General considerations, IMA J. Appl. Math. **6**, 76 (1970).

[35] R. Fletcher, A new approach to variable metric algorithms, Comput. J. **13**, 317 (1970).

[36] D. Goldfarb, A family of variable-metric methods derived by variational means, Math. Comp. **24**, 23 (1970).

[37] D. F. Shanno, Conditioning of quasi-newton methods for function minimization, Math. Comp. **24**, 647 (1970).

[38] J. E. Dennis Jr. and R. B. Schnabel, *Numerical Methods for Unconstrained Optimization and Nonlinear Equations* (SIAM, Philadelphia, 1996).

[39] M. A. Ortigoza, M. Aminpour, and T. S. Rahman, Thermal expansion at a metal surface: A study of Mg(0001) and Be(10-10), Surf. Sci. **632**, 14 (2015).

[40] P. Blaha, K.Schwarz, R. L. F. Tran, G. Madsen, and L. Marks, WIEN2k: An APW+lo program for calculating the properties of solids, J. Chem. Phys. **152**, 074101 (2020).

[41] Y. Zhong, K. Ozturk, J. O. Sofo, and Z.-K. Liu, Contribution of first-principles energetics to the Ca–Mg thermodynamic modeling, J. Alloys Compd. **420**, 98 (2006).

[42] F. Tran, L. Kalantari, B. Traoré, X. Rocquefelte, and P. Blaha, Nonlocal van der Waals functionals for solids: Choosing an appropriate one, Phys. Rev. Mater. **3**, 063602 (2019).

[43] C. B. Walker and M. Marezio, Lattice parameters and zone overlap, Acta Metall. **7**, 769 (1959).

[44] D. K. Smith and H. R. Leider, Low-temperature thermal expansion of LiH, MgO and CaO, J. Appl. Cryst. **1**, 246 (1968).

[45] P. Haas, F. Tran, and P. Blaha, Calculation of the lattice constant of solids with semilocal functionals, Phys. Rev. B **79**, 085104 (2009).

[46] D. C. Langreth and S. H. Vosko, Response functions and nonlocal functionals, Adv. Quantum. Chem. **21**, 175 (1990).

[47] J. P. Perdew and Y. Wang, Accurate and simple density functional for the electronic exchange energy: Generalized gradient approximation, Phys. Rev. B **33**, 8800 (1986).

[48] É. D. Murray, K. Lee, and D. C. Langreth, Investigation of exchange energy density functional accuracy for interacting molecules, J. Chem. Theory Comput. **5**, 2754 (2009).

[49] J. P. Perdew, A. Ruzsinszky, G. I. Csonka, O. A. Vydrov, G. E. Scuseria, L. A. Constantin, X. Zhou, and K. Burke, Restoring the density-gradient expansion for exchange in solids and surfaces, Phys. Rev. Lett. **100**, 136406 (2008).

[50] A. D. Becke, On the large-gradient behavior of the density functional exchange energy, J. Chem. Phys. **85**, 7184 (1986).

[51] W. Tyson and W. Miller, Surface free energies of solid metals: Estimation from liquid surface tension measurements, Surf. Sci. **62**, 267 (1977).

[52] P. T. Sprunger, K. Pohl, H. L. Davis, and E. W. Plummer, Multilayer relaxation of the Mg(0001) surface, Surf. Sci. **297**, L48 (1993).

[53] F. R. de Boer, R. Boom, W. C. M. Mattens, A. R. Miedema, and A. K. Niessen, *Cohesion in Metals: Transition Metal Alloys* (North-Holland, Amsterdam, 1988).

[54] Ismail, P. Hofmann, A. P. Baddorf, and E. W. Plummer, Thermal expansion at a metal surface: A study of Mg(0001) and Be(10-10), Phys. Rev. B **66**, 245414 (2002).

[55] G. Kresse and J. Furthmüller, Efficient iterative schemes for ab initio total-energy calculations using a plane-wave basis set, Phys. Rev. B **54**, 11169 (1996).

[56] L. Bengtsson, Dipole correction for surface supercell calculations, Phys. Rev. B **59**, 12301 (1999).

[57] S. Neppl and O. Gessner, Time-resolved X-ray photoelectron spectroscopy techniques for the study of interfacial charge dynamics, J. Electron Spectrosc. Relat. Phenom. **200**, 64 (2015).

[58] S.-H. Jang and S. F. Chichibu, Structural, elastic, and polarization parameters and band structures of wurtzite ZnO and MgO, J. Appl. Phys. **112**, 073503 (2012).